Check for updates

View Article Online
View Journal

Dalton Transactions

An international journal of inorganic chemistry

Accepted Manuscript

This article can be cited before page numbers have been issued, to do this please use: K. Lemoine, R. Moury, J. Lhoste, A. Ribaud, M. Leblanc, J. Grenèche, J. Tarascon and V. Maisonneuve, *Dalton Trans.*, 2020, DOI: 10.1039/D0DT01310B.

This is an Accepted Manuscript, which has been through the Royal Society of Chemistry peer review process and has been accepted for publication.

Accepted Manuscripts are published online shortly after acceptance, before technical editing, formatting and proof reading. Using this free service, authors can make their results available to the community, in citable form, before we publish the edited article. We will replace this Accepted Manuscript with the edited and formatted Advance Article as soon as it is available.

You can find more information about Accepted Manuscripts in the Information for Authors.

Please note that technical editing may introduce minor changes to the text and/or graphics, which may alter content. The journal's standard Terms & Conditions and the Ethical guidelines still apply. In no event shall the Royal Society of Chemistry be held responsible for any errors or omissions in this Accepted Manuscript or any consequences arising from the use of any information it contains.

ROYAL SOCIETY OF CHEMISTRY

rsc.li/dalton

View Article Online
DOI: 10.1039/C9DT01310B

Stabilization of a mixed iron vanadium based Hexagonal Tungsten Bronze hydroxyfluoride HTB-$(Fe_{0.55}V_{0.45})F_{2.67}(OH)_{0.33}$ as positive electrode for lithium-ion batteries

Kévin Lemoine,[a] Romain Moury,[a] Jérôme Lhoste,[a] Annie Hémon-Ribaud,[a] Marc Leblanc,[a] Jean-Marc Grenèche,[a] Jean-Marie Tarascon,[b,c] Vincent Maisonneuve[a*]

[a] Institut des Molécules et des Matériaux du Mans, UMR 6283 CNRS, Le Mans Université, Avenue Olivier Messiaen, 72085 Le Mans Cedex 9, France

[b] Collège de France, Chaire de Chimie du Solide et de l'Energie, UMR 8260 CNRS, 11 Place Marcelin Berthelot, 75231 Paris, France

[c] Réseau sur le Stockage Electrochimique de l'Energie (RS2E), FR CNRS 3459, 80039 Amiens, France

Kévin Lemoine present address: Department of Chemistry, Faculty of Science, Gakushuin University, 1-5-1 Mejiro, Toshima-ku, Tokyo 171-8588, Japan

Published on 13 May 2020. Downloaded by Uppsala University on 5/14/2020 8:40:24 AM.

Dalton Transactions Accepted Manuscript

Abstract

In our search for novel insertion compounds for Li-based batteries, we have identified a new mixed iron vanadium based Hexagonal Tungsten Bronze (HTB) type phase. Its synthesis involves two steps which consist first of preparing the mixed metal hydrate fluoride $Fe_{1.64}V_{1.36}F_8(H_2O)_2$ by a microwave assisted thermal process, followed by a thermal treatment under air to obtain the metastable HTB-

View Article Online
DOI: 10.1039/D0DT01310B

$(Fe_{0.55}V_{0.45})F_{2.67}(OH)_{0.33}$ hydroxyfluoride. ^{57}Fe Mössbauer spectrometry demonstrates the presence of oxidation states Fe^{2+} and Fe^{3+} in $Fe_{1.64}V_{1.36}F_8(H_2O)_2$ as opposed to only Fe^{3+} in HTB-$(Fe_{0.55}V_{0.47})F_{2.67}(OH)_{0.33}$. Moreover Mössbauer spectra recorded at 77 K reveal that none of the compounds shows magnetic ordering owing to the presence of V^{3+} distributed over the crystallographic sites of Fe^{3+}. Complementary X-ray spectroscopy and Rietveld refinement further confirm the successful synthesis of HTB-$(Fe_{0.55}V_{0.45})F_{2.67}(OH)_{0.33}$. Electrochemically-wise, the new HTB-$(Fe_{0.55}V_{0.45})F_{2.67}(OH)_{0.33}$ shows a first discharge capacity of 181 mAh.g^{-1} with 67% of this capacity remaining upon cycling. Unlike HTB-$FeF_{2.66}(OH)_{0.34}$ the structure remains stable after the first discharge confirming the positive effect of the vanadium in the HTB network.

1. Introduction

Improving both the energy density and power rate of present Li-ion batteries together with their sustainability while preserving safety is nowadays a major research challenge.[1,2] To achieve this goal, hope is placed on all-solid-state batteries, which by virtue of using a Li metal negative electrode and a solid electrolyte could lead to both

Published on 13 May 2020. Downloaded by Uppsala University on 5/14/2020 8:40:24 AM.

Dalton Transactions Accepted Manuscript

View Article Online
DOI: 10.1039/D0DT01310B

energy density and safety improvements, respectively. However, interface problems remain to be solved prior such an option could become a practical reality. Meanwhile, the $LiFePO_4$-based lithium-metal-polymer battery technology presently on the market provides a midway solution since it enhances safety owing to the use of a solvent-free PEO polymeric membrane.[3-5] In contrast, this technology does not fully capitalize on the use of Li negative electrode, which must be in large excess because of some dead mossy Li forming upon cycling. Furthermore, it is penalized by its mandatory operation at 55°C to reach sufficient ion conduction in the electrolyte for ensuring good performances. As a whole, besides enhancing the coulombic plating-stripping efficiency of the Li-electrode another way to enhance the energy of Li-polymer batteries is to design better positive electrodes bearing in mind that they can be Li-free content, as opposed to the Li-ion technology, since they use a Li negative electrode. Let us simply recall that Li-free V_2O_5 was the positive electrode material early used in the development of Li-polymer batteries, thus a greater opening of the materials field to explore.

Within this context, FeF_3 with a theoretical capacity of 237 $mAh.g^{-1}$ and an anticipated high operational voltage due to the presence of the very electronegative

Published on 13 May 2020. Downloaded by Uppsala University on 5/14/2020 8:40:24 AM.

Dalton Transactions Accepted Manuscript

View Article Online
DOI: 10.1039/D0DT01310B

fluorine element has been intensively explored.[6-11] Three polymorphs exist for FeF_3. The most thermodynamically stable one adopts the rhombohedral ($R\bar{3}c$) ReO_3 type structure[12] and simultaneously shows the closest packing, hence being the most prone to limited Li^+ diffusivity. In contrast, the two other polymorphs, namely pyrochlore (Pyr-FeF_3, $Fd\bar{3}m$)[13] with 3D open network and Hexagonal Tungsten Bronze (HTB-FeF_3, $Cmcm$)[14] with 1D channels along the *c* axis, are metastable and display open frameworks.[10] These metastable structures can be synthesized with water molecules within the framework.[15] Recently, we have succeeded in preparing a water-free (HTB-$FeF_{2.67}(OH)_{0.33}$) by thermal dehydration of $Fe_3F_8(H_2O)_2$ which exhibits an experimental capacity of 170 mAh.g^{-1} vs. Li^+/Li.[16] Following this strategy, we have also explored the effect of mixing 3d transition metals (TM) on the electrochemical properties of new amorphous oxyfluorides obtained by thermal treatment of the hydrated $M^{2+}Fe^{3+}{}_2F_8(H_2O)_2$ (M^{2+} = Mn, Co, Ni, Cu) and found attractive electrochemical properties.[17,18] The iron-vanadium hydrated fluoride $Fe_{1.64}V_{1.36}F_8(H_2O)_2$ was studied as well and interestingly, we showed that during its thermal decomposition an intermediate phase is formed with HTB structure type. The hydrate adopts the monoclinic *C2/m* $Fe_3F_8(H_2O)_2$ structure type which is built up from

Published on 13 May 2020. Downloaded by Uppsala University on 5/14/2020 8:40:24 AM.

Dalton Transactions Accepted Manuscript

View Article Online
DOI: 10.1039/D0DT01310B

HTB sheets (**Figure 1a**). Its 3D structure can be described by perovskite layers $_{\infty}[M^{\beta+}F_4]$ connected to each other by isolated $M^{2+}{}_2F_4(H_2O)_2$ octahedra (**Figure 1b**).[19,20] At this stage, we should recall that vanadium trifluorides were only found in ReO_3 and pyrochlore packing[12,21] and that were tested as a cathode material in LIB and NIB batteries.[6,22] Herein we report on the microwave assisted solvothermal synthesis of $Fe_{1.64}V_{1.36}F_8(H_2O)_2$ followed by a proper thermal treatment to unravel the first example of mixed iron vanadium based fluoride $(Fe_{0.55}V_{0.45})F_{2.67}(OH)_{0.33}$ with a framework HTB. We precisely defined its formulation and structure from combined XRD Rietveld refinements, thermogravimetric measurements (TGA), Energy Dispersive X-ray spectroscopy (EDX), and Mössbauer spectrometry, while its electrochemical activity towards Li^+ (181 mAh.g^{-1}) was deduced by assembling HTB-$(Fe_{0.55}V_{0.45})F_{2.67}(OH)_{0.33}$/Li cells.

Published on 13 May 2020. Downloaded by Uppsala University on 5/14/2020 8:40:24 AM.

Dalton Transactions Accepted Manuscript

View Article Online
DOI: 10.1039/D0DT01310B

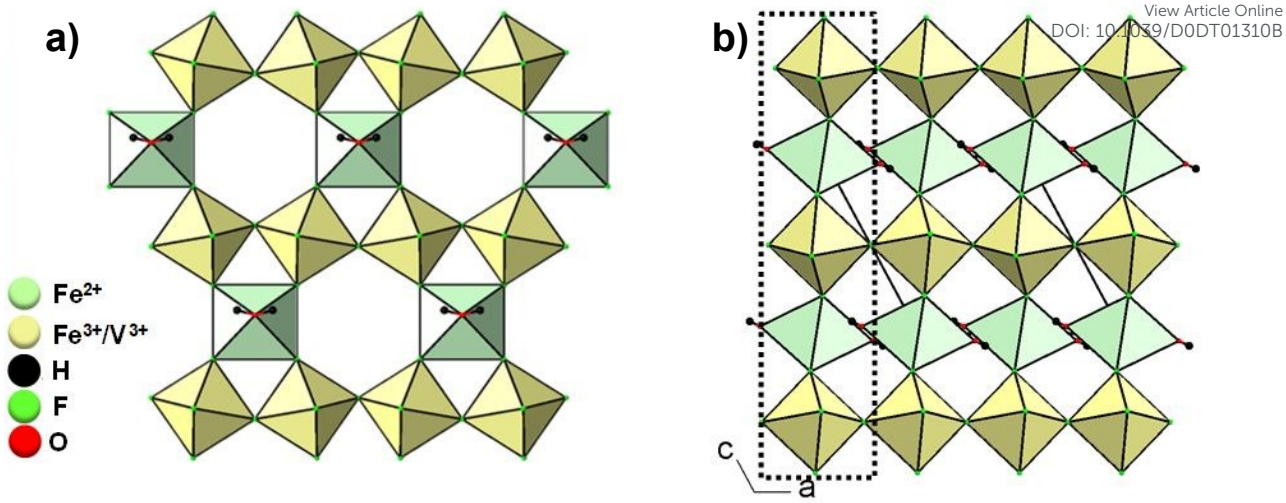

Figure 1. View of the HTB sheet (a) and projection along b of the structure of $Fe_{1.6}V_{1.4}F_8(H_2O)_2$ (b).

2. Methodology

2.1 Experimental Methods

The mixed metal fluoride $Fe_{1.64}V_{1.36}F_8(H_2O)_2$ is synthesized by solvothermal reaction using a MARS-5 microwave Digestion System (CEM Corp.) from the starting reactants $FeCl_2{\cdot}4H_2O$ (98%, Alfa Aesar), VCl_3 (Alfa Aesar), absolute methanol (99.8%, Sigma Aldrich), deionized water and hydrofluoric acid solution "HF" (27.6 mol.L^{-1}, 48%, Riedel De Haen). The safe use of highly hazardous concentrated HF solutions requires wearing gloves (neoprene) and handling inside a fume hood. The concentration [Fe^{2+}] + [V^{3+}] was fixed equal to 0.1 mol.L^{-1} and the Fe^{2+}/V^{3+}/HF/MeOH

Published on 13 May 2020. Downloaded by Uppsala University on 5/14/2020 8:40:24 AM.

Dalton Transactions Accepted Manuscript

View Article Online
DOI: 10.1039/D0DT01310B

ratio equal to 1/2/44/699. The mixture was inserted in Teflon autoclaves and stirred for 30 min then heated at 160°C for 1 h with stirring. After cooling, the light brown powder product was filtered, washed with 2 mL of ethanol and dried overnight under air at 100°C. A partial oxidation of Fe^{2+} into Fe^{3+} ions due to the presence of water leads to the formulation $Fe^{2+}Fe^{3+}_{0.64}V^{3+}_{1.36}F_8(H_2O)_2$. This product was then inserted in a furnace under ambient air and heated at 280°C, during 1 h (heating/cooling rate of 2°C/min). After cooling to room temperature, a dark brown hydroxyfluoride resulted with the formulation $(Fe_{0.55}V_{0.45})F_{2.67}(OH)_{0.33}$. It is also worth to emphasize that after the thermal treatment; all the phases are immediately outgassed at ambient temperature under secondary vacuum ($P < 10^{-5}$ bar) and stored in a glove box prior being characterized.

2.2 Characterization Methods

2.2.1 Structural and chemical compositions

X-ray diffraction patterns were collected in the range 8° ≤ 2θ ≤ 150° on a Panalytical MPD-PRO diffractometer equipped with a linear X'celerator detector with CuK_α (1.541 Å). In some cases, the CoK_α radiation (1.789 Å) was used to avoid the X-ray

Published on 13 May 2020. Downloaded by Uppsala University on 5/14/2020 8:40:24 AM.

Dalton Transactions Accepted Manuscript

View Article Online
DOI: 10.1039/D0DT01310B

fluorescence. Rietveld refinements were performed by using the Fullprof profile refinement program.[23,24] For the temperature dependant diffraction the Anton Parr reactor chamber XRK 900 heating device was used with an alumina sample holder, the temperature was allowed to equilibrate for 15 min prior to the measurement.

^{57}Fe Mössbauer measurements were performed in transmission geometry with a 925 MBq γ-source of ^{57}Co/Rh mounted on a conventional constant acceleration drive. The velocity of the source was calibrated using α-Fe as the standard at RT. The samples with 5 mg Fe/cm^2 were prepared from a softly milled powder. Data were fitted using the MOSFIT program[25] involving quadrupolar components with lorentzian lines. The isomer shift values are referred to that of α-Fe at RT.

SEM images of the powders were obtained using a JEOL microscope (JSM 6510 LV). Acceleration voltages varied between 20 and 30 kV as a function of the analyzed samples. Elementary quantitative microanalyses were performed using an Energy Dispersive X-ray (EDX) OXFORD detector with Aztec software.

2.2.2 Thermal analyses

Published on 13 May 2020. Downloaded by Uppsala University on 5/14/2020 8:40:24 AM.

Dalton Transactions Accepted Manuscript

View Article Online
DOI: 10.1039/D0DT01310B

Published on 13 May 2020. Downloaded by Uppsala University on 5/14/2020 8:40:24 AM.

Dalton Transactions Accepted Manuscript

The thermogravimetric (TGA) experiments were carried out with a thermoanalyzer SETARAM TGA 92 with a heating rate of 2°C.min^{-1} from room temperature up to 900°C under ambient air and dry air (Alphagaz, mixture of oxygen (20%) with nitrogen (80%), H_2O < 3 ppm).

X-ray thermodiffraction (HT-XRD) experiments were performed under dry air flow in an Anton Parr XRK 900 high temperature furnace with the diffractometer already described. The samples were heated from 40°C to 600°C at a heating rate of 10°C min^{-1}. X-ray diffraction patterns were recorded in the 5-60° range with a scan time of 10 min at 10°C intervals from room temperature to 400°C and 50°C intervals from 400°C to 600°C.

The powder of $Fe^{2+}Fe^{3+}_{0.64}V_{1.36}F_8(H_2O)_2$, was heated in a furnace (Nabertherm LT 3/12/P330) at a heating rate of 3°C.min^{-1} from room temperature to T ≤ 300°C under ambient atmosphere and were cooled at room temperature. Then, IR spectra were collected *ex-situ* (20°C intervals) between 40 cm^{-1} and 4000 cm^{-1} with a scan time of 2 min with an ALPHA FT-IR Spectrometer.

2.2.3 Electrochemistry characterizations

View Article Online
DOI: 10.1039/D0DT01310B

The electrochemical activity against lithium was evaluated using a Swagelok Li metal cell. Electrodes were composed of 80% active materials and 20% carbon-SP (super pure) as the conductive agent; they were ball-milled using a SPEX Miller 800 at 875 cycles/min for 15 minutes. The area of the electrode was 1 cm^2 with a loading mass of 8 mg. The electrolyte was the commercial LP30 (1M $LiPF_6$). The cell was cycled between 2 and 4 V versus Li^+/Li at C/20 current density.

2. Results and discussion

2.1. Synthesis and characterization of the hydrated fluoride

Our group recently developed a new solvothermal method assisted by microwave heating to synthesize under mild conditions pure hydrated fluorides of general formulae *M*$Fe_2F_8(H_2O)_2$.[17] Herein we implemented this strategy for the preparation of the mixed 3d TM starting with a ratio Fe^{2+}:V^{3+} of 1:2. The as-synthesized hydrate fluoride was studied by ^{57}Fe Mössbauer spectrometry to establish the Fe valence states (**Figure 2a**). The spectrum collected at 300 K can be clearly interpreted as a quadrupolar hyperfine structure with two paramagnetic components consisting of well resolved doublets with Lorentzian profiles. The asymmetrical profile of the right line

Published on 13 May 2020. Downloaded by Uppsala University on 5/14/2020 8:40:24 AM.

Dalton Transactions Accepted Manuscript

View Article Online
DOI: 10.1039/C9DT01310B

corresponding to the ferrous component can solely be fitted with two quadrupole doublets, resulting from disordered chemical atomic environments. The refined (mean) values of the characteristic hyperfine parameters (**Table 1**) reveal clearly both valence states Fe^{2+} and Fe^{3+}, with a molar ratio Fe^{3+}/Fe^{2+} = 0.64.

Published on 13 May 2020. Downloaded by Uppsala University on 5/14/2020 8:40:24 AM.

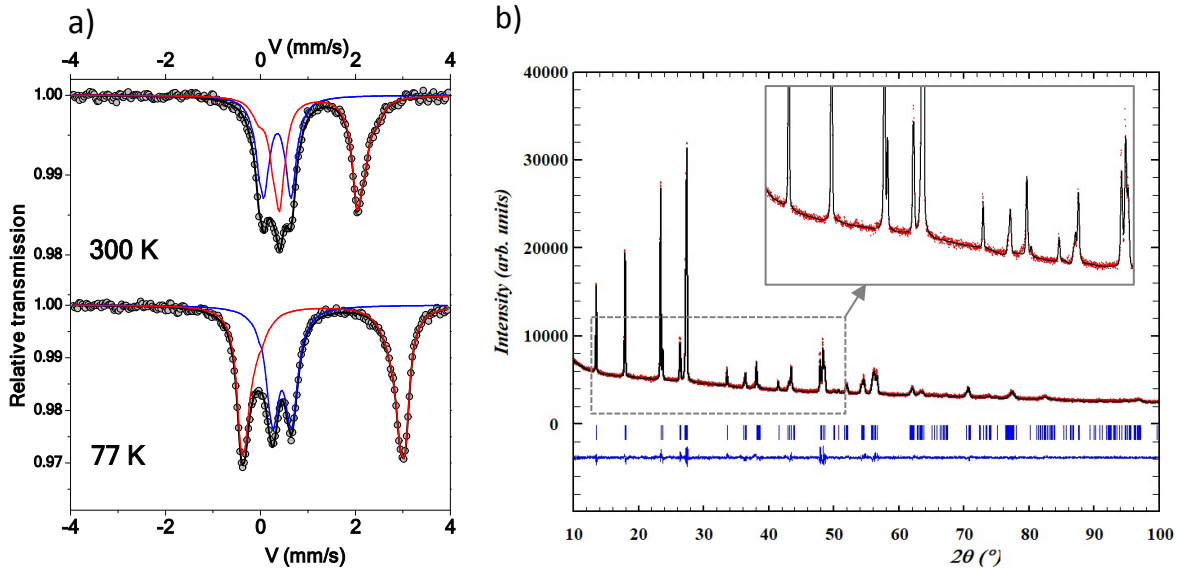

Figure 2. ^{57}Fe Mössbauer spectra recorded at 300 K and 77 K on $Fe_{1.64}V_{1.36}F_8(H_2O)_2$; the red line corresponds to Fe^{2+} and the blue line to Fe^{3+} (a), Rietveld refinement of the structural model with the diffraction pattern (b) of $Fe_{1.64}V_{1.36}F_8(H_2O)_2$ at room temperature.

Interestingly, the spectrum recorded at 77 K does not reflect the expected magnetic order previously observed for Fe^{3+} below 157 K in $M^{2+}Fe^{3+}{}_2F_8(H_2O)_2$ phases, with the

Dalton Transactions Accepted Manuscript

View Article Online
DOI: 10.1039/D0DT01310B

typical splitting in Zeeman sextet. Instead, it shows two paramagnetic components, confirming the analysis made on the 300 K spectrum. *A priori*, the presence of V^{3+} on Fe^{3+} crystallographic sites explains the magnetic order reduction, namely the weakening of the Fe-Fe interactions by the presence of V^{3+} ions. Consequently, instead of the expected formulation $Fe^{2+}V^{3+}{}_2F_8(H_2O)_2$ we obtained $Fe^{2+}Fe^{3+}{}_{0.64}V^{3+}{}_{1.36}F_8(H_2O)_2$ denoted $Fe_{1.64}V_{1.36}F_8(H_2O)_2$ hereafter. In fact, during the synthesis, part of Fe^{2+} is oxidized to Fe^{3+} due to the water content in aqueous HF.

Table 1. Refined values of hyperfine parameters of $Fe_{1.64}V_{1.36}F_8(H_2O)_2$ phase at 300 K and 77 K

Temperature		Fe^{n+}	δ ± 0.01	ΔE_Q ± 0.01	τ ± 0.01
300 K	2 doublets	Fe^{3+}	0.46	0.58	0.39
		Fe^{2+}	<1.33>	<1.74>	0.61
77 K	2 doublets	Fe^{3+}	0.57	0.40	0.39
		Fe^{2+}	<1.45>	<3.09>	0.61

δ and ΔE_Q are given in $mm.s^{-1}$

Diffraction pattern recorded on the as-synthesized phase reveals a structure isotypic to $Fe_3F_8(H_2O)_2$ that can be indexed with the $C2/m$ space group. Rietveld refinement was performed using the atomic positions of $Fe_3F_8(H_2O)_2$ (ISCD-38366); the

Published on 13 May 2020. Downloaded by Uppsala University on 5/14/2020 8:40:24 AM.

Dalton Transactions Accepted Manuscript

View Article Online
DOI: 10.1039/D0DT01310B

occupancy factor for the shared 4f Wyckoff position for Fe^{3+} and V^{3+} was fixed by using the Mössbauer spectrometry results. 4f Wyckoff position for V^{3+} have been chosen considering bond valence calculations (**Table S3**), and careful inspection of M-(O/Ow/F) distances. A reliable fit with acceptable agreement factors (R_B/R_f = 0.039/0.057) was obtained (**Figure 2b)**. Structural parameters obtained after refinement are gathered in **Tables S1** and **S2**.

2.2. Thermal decomposition

The precursor $Fe_{1.64}V_{1.36}F_8(H_2O)_2$ was then subjected to thermal treatment and its structural and water content evolutions were followed by *in situ* XRD and TGA analysis. **Figure 3a** displays the thermodiffractograms obtained on the hydrated phase, it can be seen that this phase is stable up to 220 °C, and starts its dehydration at 240°C giving the formulation stated now and discussed later HTB-$(Fe_{0.55}V_{0.45})F_{2.67}(OH)_{0.33}$. The temperature range of stability for this HTB hydroxyfluoride is between 240 and 280°C. Above 280°C a mixture between HTB and a new unknown phase up to 400°C is observed (Figure S1) and at 500°C only hematite Fe_2O_3 is left. Owing to the absence of vanadium based crystalline phase

Published on 13 May 2020. Downloaded by Uppsala University on 5/14/2020 8:40:24 AM.

Dalton Transactions Accepted Manuscript

View Article Online
DOI: 10.1039/D0DT01310B

above 500°C we can suggest the sublimation of a vanadium phase like VOF_3, with sublimation temperature of 480°C, or VF_3.[26] The thermogravimetric measurement (**Figure 3b**) shows a total weight loss of 63.8 % starting above 200°C. Combining the previous thermal analysis with HT-XRD, the following decomposition reactions can be suggested. Equation (1) is valid in the temperature range [220-280°C] and Equation (2) in the range [280-500°C].

$$Fe_{1.64}V_{1.36}F_8(H_2O)_2 + 1/4O_2 \rightarrow 3(Fe_{0.55}V_{0.45})F_{2.67}(OH)_{0.33} + 3/2H_2O \quad (1)$$

$$Fe_{0.55}V_{0.45}F_{2.67}(OH)_{0.33} + 0.495H_2O \rightarrow 0.45VF_3 + 0.275Fe_2O_3 + 1.32HF \quad (2)$$

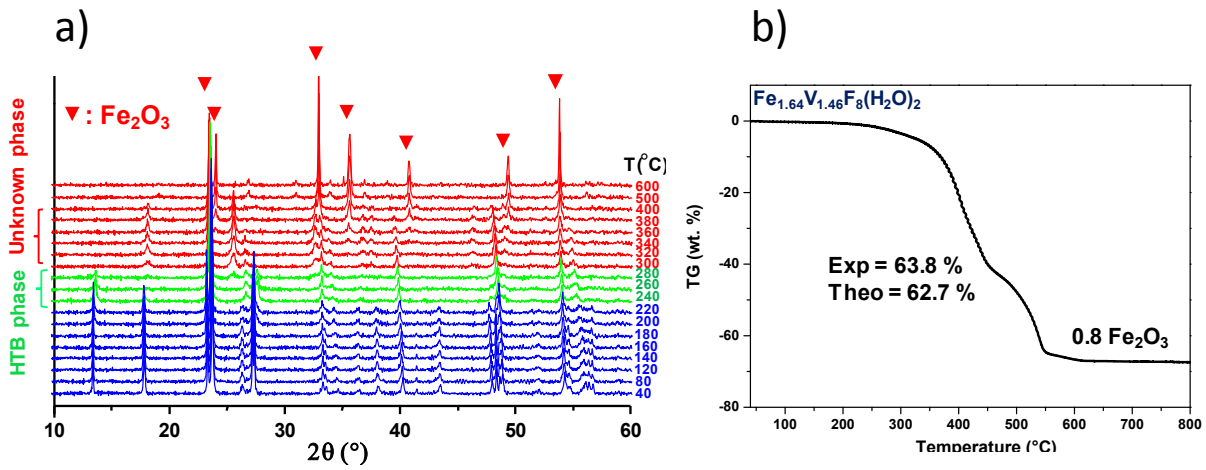

Figure 3. Thermal evolution of X-ray diffraction patterns (Cu Kα) under dry air (a) and thermogravimetric curve under dry air (b) of $Fe_{1.6}V_{1.4}F_8(H_2O)_2$.

Published on 13 May 2020. Downloaded by Uppsala University on 5/14/2020 8:40:24 AM.

Dalton Transactions Accepted Manuscript

View Article Online
DOI: 10.1039/D0DT01310B

Despite a narrow temperature window of stability, the HTB-phase was successfully isolated by heating the hydrated fluoride during 1 h at 280°C under ambient air. In order to follow the dehydration process, *ex situ* FTIR experiment at different temperatures were performed (**Figure S2**). The FTIR spectrum at 160°C presents two bands: one broad, between 3000 and 3500 cm^{-1} corresponding to OH stretching modes and one sharp at 1625 cm^{-1} characteristic of water bending mode. As the temperature increases, these absorption bands decrease, confirming water removal, while two new intense peaks at 1090 and 1170 cm^{-1} raise. These bands are attributed to hydroxyl deformation bands that involve metal oxygen bonds. Vimont *et al.* have demonstrated that these bands are a coupling of in-plane bending δ(OH) and v(M-O) vibration in HTB metal hydroxyfluorides.[27] These results would evidence the formation of a metal hydroxyfluoride.

Mössbauer experiments were carried out at 300 K and 77 K on the as-obtained phase to determine the valence states and the environment of ^{57}Fe (**Figure 4a**) after the thermal treatment. The spectra consist of a single broadened and asymmetrical line which can be perfectly described by means of two main paramagnetic doublets plus a minor doublet corresponding to FeF_2 impurity (2 mol%). The refined values of

Published on 13 May 2020. Downloaded by Uppsala University on 5/14/2020 8:40:24 AM.

Dalton Transactions Accepted Manuscript

View Article Online
DOI: 10.1039/D0DT01310B

the hyperfine parameters, summarized in **Table 2**, reveal the presence of only one valence state for Fe^{3+} in two different environments. Because the crystallographic structure consists only of octahedral units, the significantly different values of the isomer shift suggest different chemical environments: the first environment with the smallest quadrupole splitting (0.24 $mm.s^{-1}$) and the highest isomer shift (0.48 $mm.s^{-1}$) corresponds to a regular FeF_6 octahedron whereas the second one, with the quadrupole splitting of 0.70 $mm.s^{-1}$ and a weaker isomer shift (0.39 $mm.s^{-1}$) is attributed to an asymmetric octahedron with either hydroxide or fluorine at the vertexes.[16,28,29]

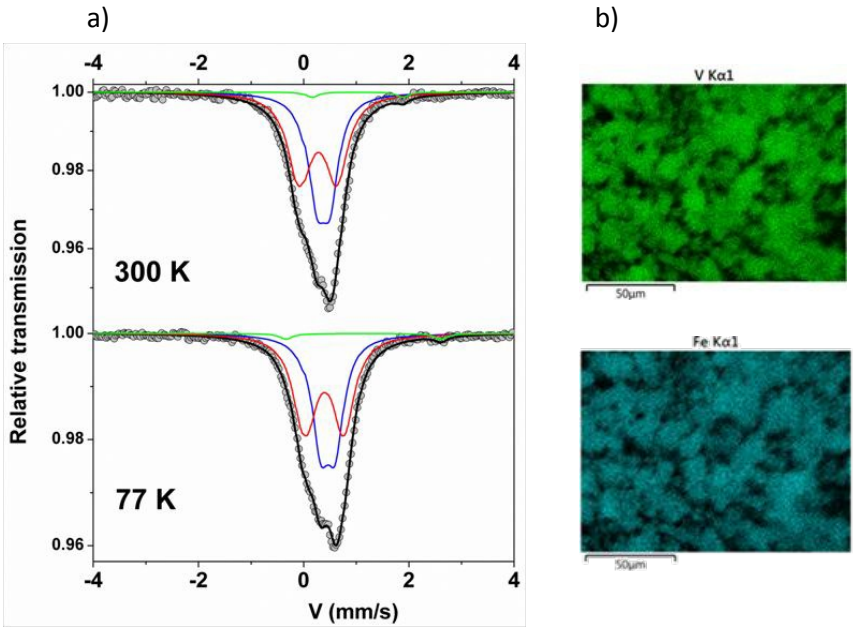

Published on 13 May 2020. Downloaded by Uppsala University on 5/14/2020 8:40:24 AM.

Dalton Transactions Accepted Manuscript

View Article Online
DOI: 10.1039/D0DT01310B

Figure 4. ^{57}Fe Mössbauer spectra recorded at 300 K and 77 K on HTB-$(Fe_{0.55}V_{0.45})F_{2.67}(OH)_{0.33}$, (a) and EDX elemental mapping of HTB-$(Fe_{0.55}V_{0.45})F_{2.67}(OH)_{0.33}$ (b).

The reported magnetic order temperature for fluorides having the HTB type structure alike FeF_3 is of ≈ 97 K whereas in our experiment, the spectrum at 77 K exhibits only two paramagnetic components, meaning that the magnetic order temperature is lowered.[15,30] This feature would confirm the presence of V^{3+} on Fe^{3+} crystallographic sites. To discard phase segregation which would corroborate the atomic distribution between V^{3+} and Fe^{3+}, EDX spectroscopy on the stabilized HTB hydroxyfluoride was performed by SEM (**Figure 4b**). A homogenous dispersion of both metals without phase segregation was noticed with Fe^{3+}/V^{3+} ratio close to 1.

Table 2. Refined values of the hyperfine parameters of $Fe_{0.55}V_{0.45}F_{2.67}(OH)_{0.33}$ at 300 K and 77 K.

Temperature		Fe^{n+}	δ ± 0.01	ΔE_Q ± 0.01	τ ± 0.01
300 K	3 doublets	Fe^{3+}	0.48	0.24	0.39
			0.39	0.70	0.59
		Fe^{2+}	1.15	1.72	0.02

Published on 13 May 2020. Downloaded by Uppsala University on 5/14/2020 8:40:24 AM.

Dalton Transactions Accepted Manuscript

View Article Online
DOI: 10.1039/D0DT01310B

		Fe^{3+}	0.57	0.26	0.39
77 K	3 doublets		0.51	0.71	0.59
		Fe^{2+}	1.25	2.92	0.02

δ and ΔE_Q are given in $mm.s^{-1}$

A diffraction pattern was recorded on the stabilized phase to confirm the mixed iron vanadium based HTB type structure (**Figure 5a**). The pattern was indexed using $P6_3/m$ instead of the original space group $Cmcm$ for HTB-FeF_3 (**Table S3**) in order to better estimate the Fe-F distances, as described by Leblanc *et al.* and further confirmed by Lemoine *et al.*[16,31] Rietveld refinement was performed with V^{3+} sharing the 6g Wyckoff position of Fe^{3+} (Mössbauer result) and with a partial occupancy of the 12i Wyckoff position of fluorine atoms F(2) by oxygen atoms fixed at 16.7% to comply with the OH/F ratio established by TGA, structural parameters are gathered in **Table 3.** The occupancy of V^{3+} and Fe^{3+} on 6g Wyckoff positions was fixed with respect to Equation 1. As HTB structure easily absorbs water during sample preparation, we added water molecules within the hexagonal channels on the Wyckoff position 2a, giving satisfactory fit with agreement factors (R_B/R_f = 0.086/0.099). A lack of intensity is observed on (002) (2θ = 27.4°) reflection possibly due to either preferred orientation or to the high degree of freedom of water

Published on 13 May 2020. Downloaded by Uppsala University on 5/14/2020 8:40:24 AM.

Dalton Transactions Accepted Manuscript

View Article Online
DOI: 10.1039/DDT01310B

displacement within the cavity. Structural parameters after refinement are gathered in **Table 4**. FTIR, Mössbauer spectrometry, EDXS and XRD confirm the successful stabilization of the first vanadium based fluoride HTB type structure (**Figure 5b**).

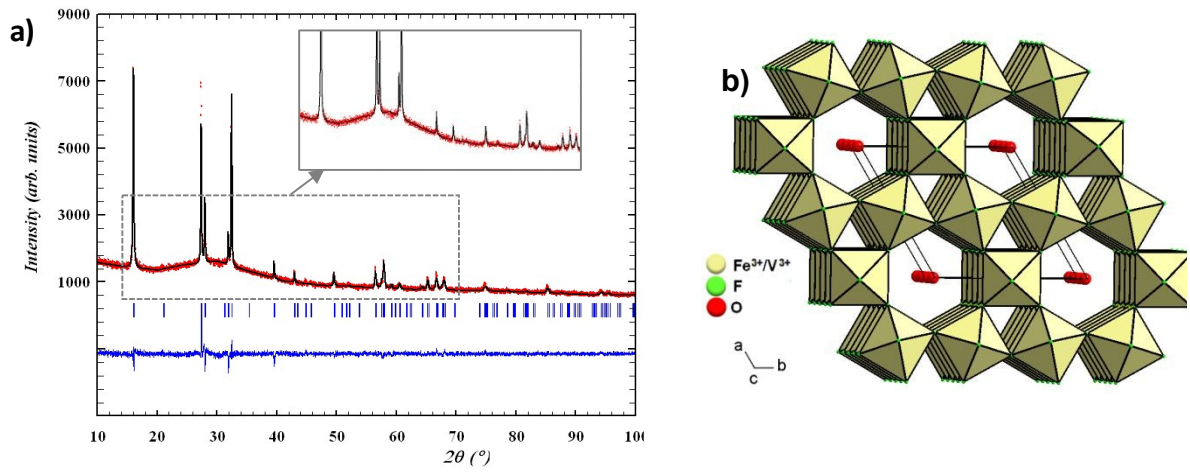

Figure 5. Rietveld refinement of the structural model with the diffraction pattern (Co Kα_1 Kα_2) (a) and view of structure (b) of HTB-$(Fe_{0.55}V_{0.45})F_{2.67}(OH)_{0.33}\cdot nH_2O$.

Table 3. Data collection and structural parameters of HTB-$(Fe_{0.55}V_{0.45})F_{2.67}(OH)_{0.33}\cdot nH_2O$ obtained by powder diffraction.

Formulation	$(Fe_{0.55}V_{0.45})F_{2.67}(OH)_{0.33}\cdot 0.1H_2O$	Distances (Å)
System / Space Group	hexagonal / $P6_3/m$	2x (Fe/V)-F(1) = 1.89(1)
a (Å), c (Å)	7.391(1), 7.557(1)	
V (Å^3), Z	357.5(1), 6	2 x (Fe/V)-F(2)/O(2) = 1.91(9)
Wavelength (Å)	CoK_α	2 x (Fe/V)-F(2)/O(2) = 1.94(13)
$\rho_{calc.}$ (g.cm^{-3})	3.081	Ow-F(1)/O(1) = 3.26(8)
2θ (°)	5 – 150	
Unique refl.	366	**Valence**

Published on 13 May 2020. Downloaded by Uppsala University on 5/14/2020 8:40:24 AM.

Dalton Transactions Accepted Manuscript

View Article Online
DOI: 10.1039/D0DT01310B

Refined param.	15	ΣV(1)/Fe(1) = +3.31
R_p / R_{wp}	0.436 / 0.251	
R_B / R_f	0.084 / 0.081	
χ^2	2.13	

Published on 13 May 2020. Downloaded by Uppsala University on 5/14/2020 8:40:24 AM.

Dalton Transactions Accepted Manuscript

Table 4. Atomic positions and isotropic displacement parameters of HTB-$(Fe_{0.55}V_{0.45})F_{2.67}(OH)_{0.33}\cdot 0.1H_2O$.

Atome	Site	x	y	z	τ	B_{eq} (Å^2)
Fe(1)	6g	½	0	0	0.546	1.7(1)
V(1)	6g	½	0	0	0.454	1.7(1)
F(1)	6h	0.505(5)	-0.017(4)	¼	1	4.6(3)
F(2)	12i	0.210(13)	-0.206(13)	-0.001(5)	0.833	4.6(3)
O(2)	12i	0.210(13)	-0.206(13)	-0.001(5)	0.167	4.6(3)
Ow(1)	2a	0	0	¾	0.30	6.9(1)

τ stands for occupancies

2.3. Electrochemical evaluation

Cylic voltammetry charge-discharge measurements were performed on Li-half cells using either the hydrated fluoride or the HTB hydroxyfluoride as the positive electrode. The cells were cycled between 2 and 4 V vs Li^+/Li at a rate of C/20 (**Figure 6**). The low cutoff voltage (2 V) was chosen to avoid irreversible conversion into metallic Fe that is known to happen in these types of phases below ≈ 1.9 V.[22] The HTB-$(Fe_{0.55}V_{0.45})F_{2.67}(OH)_{0.33}$ phase can uptake during the first discharge more than

View Article Online
DOI: 10.1039/D0DT01310B

0.7 Li^+ (e.g. ≈ 180 mAh.g^{-1}) while $Fe_{1.64}V_{1.36}F_8(H_2O)_2$ barely uptake 0.04 Li^+ (**Figure 6a**). This indicates that water molecules hinder Li^+ diffusivity within the hydrated fluoride, as already noticed.[16] Turning back to the capacity of $(Fe_{0.55}V_{0.45})F_{2.67}(OH)_{0.33}$ it drops to 123 mAh.g^{-1} and remains constant up to the 10th cycle (**Figure 6b**), the maximum we have tried. The large capacity loss (≈ 30%) between the first discharge and first charge exceeds what is usually found in intercalation compounds. Electrolyte or electrode decomposition are usually responsible for such large capacity losses, but the constancy of the capacity retention once the first cycle is achieved, does not support this explanation.[32] The diffraction pattern (**Figure 6c**) exhibits the most intense HTB peaks at 13.8, 23.5 and 27.9° for HTB-$(Fe_{0.55}V_{0.45})F_{2.67}(OH)_{0.33}$, still persisting after the discharge to 2 V with a visible shift in lower angle values especially for the peaks corresponding to the (110), (002), (130), (112) and (220) reflections attesting the lithium insertion in the structure. A broadening of these Bragg peaks results probably from an amorphization and would explain the irreversible trapping (0.2 Li^+) occurring through the first cycle. Such trapping was also evidenced in previous works on HTB-hydroxyfluoride through in situ XRD measurements[16] and PDF analyses by Dambournet *et al.* in which $FeF_{2.2}(OH)_{0.8}O_{x/2}\square_{x/2}$ collapse yielding

Published on 13 May 2020. Downloaded by Uppsala University on 5/14/2020 8:40:24 AM.

Dalton Transactions Accepted Manuscript

View Article Online
DOI: 10.1039/D0DT01310B

disordered rutile and rock salt structure types.[33,34] The remaining HTB network suggests the positive effect of vanadium in preventing the phase transition from the HTB structure to the more thermodynamically stable allotropic varieties of FeF_3[16] that was observed for $FeF_{2.67}(OH)_{0.33}$ (**Figure 6c**). Such positive effect of vanadium within the HTB structure was also studied and observed with other 3d elements like Ti,[35,36] Co[37] or Mn.[38,39]

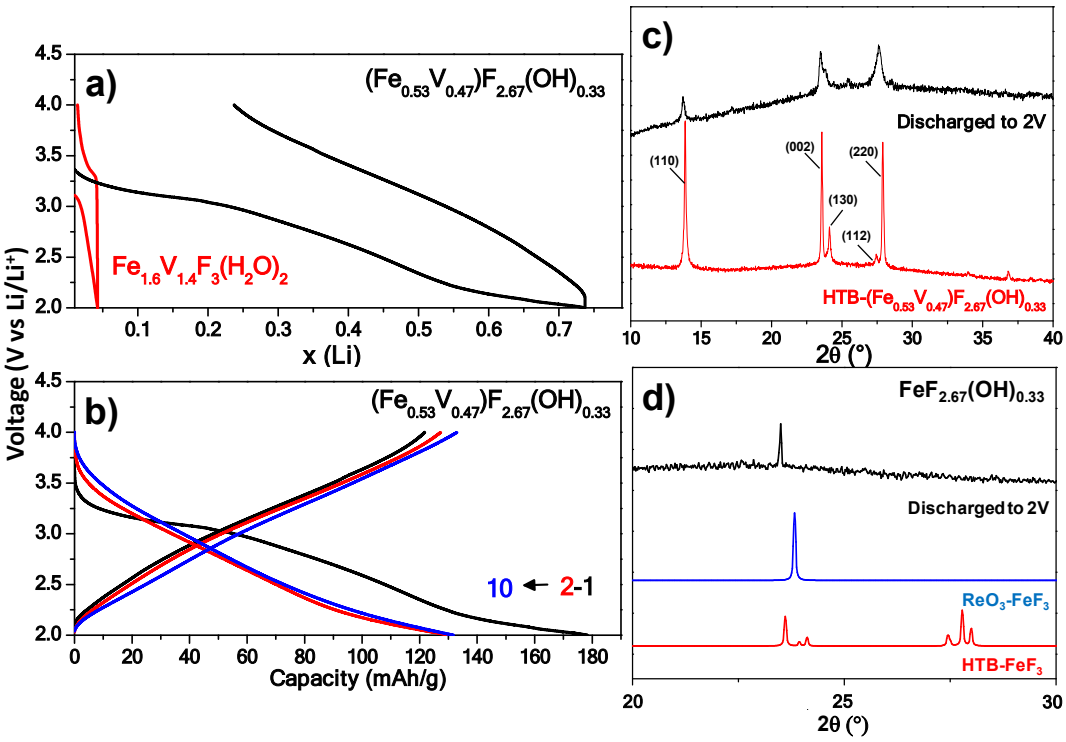

Figure 6. First discharge and charge voltammetric curves vs Li^+/Li for $Fe_{1.64}V_{1.36}F_8(H_2O)_2$ and HTB-$(Fe_{0.55}V_{0.45})F_{2.67}(OH)_{0.33}$ (a) and cyclic voltammetry curves of HTB-$(Fe_{0.55}V_{0.45})F_{2.67}(OH)_{0.33}$ (b) at C/20, XRD patterns of HTB-

Published on 13 May 2020. Downloaded by Uppsala University on 5/14/2020 8:40:24 AM.

Dalton Transactions Accepted Manuscript

View Article Online
DOI: 10.1039/D0DT01310B

$(Fe_{0.55}V_{0.45})F_{2.67}(OH)_{0.33}$ before and after the first discharge to 2 V with (hkl) indices for 13.8°, 24.7° and 27.6° Bragg peaks, (c) and HTB-$FeF_{2.67}(OH)_{0.33}$ after the first discharged to 2V compared to theoretical XRD pattern of ReO_3-FeF_3 and HTB-FeF_3 (d).

3. Conclusion

We have reported the synthesis of the first vanadium based HTB fluoride $(Fe_{0.55}V_{0.45})F_{2.67}(OH)_{0.33}$ via a controlled dehydration reaction. It crystallizes, as deduced by Rietveld refinement, in the $P6_3/m$ space group confirming the HTB type structure with hexagonal channels. The distribution of vanadium/iron at the crystallographic sites belonging to the HTB structure ($(Fe_{0.55}V_{0.45})F_{2.67}(OH)_{0.33}$) was restrained from Mössbauer spectrometry. This phase can uptake 0.7 Li^+ in discharge, of which only 0.5 can be removed in charge, the irreversibility (≈ 0.2 Li^+) having probably been most associated with partial amorphization of the structure or a reduction of the coherent diffraction domains. In addition, XRD analysis has demonstrated the advantage of vanadium in stabilizing the metastable HTB network which was partially preserved in the first discharge. An obvious extension of this work

Published on 13 May 2020. Downloaded by Uppsala University on 5/14/2020 8:40:24 AM.

Dalton Transactions Accepted Manuscript

View Article Online
DOI: 10.1039/D0DT01310B

will be to further manipulate the chemistry of this phase by selecting the appropriate cationic substituent and its correct content to stabilize HTB against its partial amorphization during discharge to take advantage of its full capacity.

Conflicts of interest

There are no conflicts to declare.

Acknowledgments

The authors acknowledge the French Research Ministry for the doctoral grant to KL and the platforms of IMMM “Diffusion et Diffraction des Rayons-X” and “Microscopy”.

Published on 13 May 2020. Downloaded by Uppsala University on 5/14/2020 8:40:24 AM.

Dalton Transactions Accepted Manuscript

View Article Online
DOI: 10.1039/D0DT01310B

References

1 J.M. Tarascon, M. Armand, *Nature*, 2001, **414**, 359-367.

2 M. Armand, J.M. Tarascon, Building better batteries, *Nature*, 2008, **451**, 652-657.

3 L. Damen, J. Hassoun, M. Mastragostino, B. Scrosati, *J. Power Sources*, 2010, **195,** 6902-6904.

4 P. Hovington, M. Lagacé, A. Guerfi, P. Bouchard, A. Mauger, C.M. Julien, M. Armand, K. Zaghib, *Nano Lett.*, 2015, **15**, 2671-2678.

5 A. Mauger, M. Armand, C.M. Julien, K. Zaghib, *J. Power Sources*, 2017, **353,** 333-342.

6 H. Arai, S. Okada, Y. Sakurai, J. I. Yamaki, *J. Power Sources*, 1997, **68**, 716-719.

7 F. Badway, F. Cosandey, N. Pereira, G.G. Amatucci, *J. Electrochem. Soc.*, 2003, **150**, A1209-A1218.

8 F. Badway, F. Cosandey, N. Pereira, G.G. Amatucci, *J. Electrochem. Soc.*, 2003, **150**, A1318-A1327.

9 M.A. Reddy, M. Fichtner, *Elsevier*, 2015, pp. 51-76.

10 D.E. Conte, N. Pinna, *Mater. Renew. Sust. Energy*, 2014, **3**, 37.

11 H. Groult, A. Tressaud, *Chem. Commun.*, 2018, **54**, 11375-11382.

12 K.H. Jack, V. Gutmann, *Acta Cryst.*, 1951, **4**, 246-249.

13 R. De Pape, G. Ferey, *Mater. Res. Bull.*,1986, **21**, 971-978.

14 C. Li, C. Yin, L. Gu, R.E. Dinnebier, X. Mu, P.A. van Aken, J. Maier, *J. Am. Chem. Soc.*, 2013, **135**, 11425-11428.

15 M. Leblanc, G. Ferey, P. Chevallier, Y. Calage, R. De Pape, *J. Solid State Chem.*, 1983, **47**, 53-58.

16 K. Lemoine, L. Zhang, D. Dambournet, J.-M. Grenèche, A. Hémon-Ribaud, M. Leblanc, O.J. Borkiewicz, J.-M. Tarascon, V. Maisonneuve, J. Lhoste, *Chem. Mater.*, 2019, **31**, 4246-4257.

17 K. Lemoine, L. Zhang, J.-M. Grenèche, A. Hémon-Ribaud, M. Leblanc, A. Guiet, C. Galven, J.-M. Tarascon, V. Maisonneuve, J. Lhoste, *J. Phys. Chem. C*, 2019, **123**, 21386-21394.

18 K. Lemoine, J. Lhoste, A. Hémon-Ribaud, N. Heidary, V. Maisonneuve, A. Guiet, N. Kornienko, *Chem. Sci.*, 2019, **10**, 9209-9218.

Published on 13 May 2020. Downloaded by Uppsala University on 5/14/2020 8:40:24 AM.

Dalton Transactions Accepted Manuscript

View Article Online
DOI: 10.1039/D0DT01310B

19 E. Herdtweck, *Z. Anorg. Allg. Chem.*, 1983, **501**, 131-136.

20 M. Leblanc, G. Ferey, Y. Calage, R. De Pape, *J. Solid State Chem.*, 1984, **53**, 360-368.

21 K. Barthelet, J. Marrot, D. Riou, G. Férey, *J. Solid State Chem.*, 2001, **162**, 266-269.

22 M. Nishijima, I.D. Gocheva, S. Okada, T. Doi, J. I. Yamaki, T. Nishida, *J. Power Sources*, 2009, **190**, 558-562.

23 A. Le Bail, H. Duroy, J.L. Fourquet, *Mater. Res. Bull.*, 1988, **23**, 447-452.

24 J. Rodríguez-Carvajal, *Physica B: Condensed Matter*, 1993, **192**, 55-69.

25 J.M. Greneche, J. Linares, F. Varret, Y. Laligant, G. Ferey, *J. Magn. Magn. Mater.*, 1988, **73**, 115-122.

26 L.E. Trevorrow, *J. Phys. Chem.*, 1958, **62**, 362-362.

27 A. Vimont, J.-C. Lavalley, L. Francke, A. Demourgues, A. Tressaud, M. Daturi, *J. Phys. Chem. B*, 2004, **108**, 3246-3255.

28 N. Louvain, A. Fakhry, P. Bonnet, M. El-Ghozzi, K. Guérin, M.-T. Sougrati, J.-C. Jumas, P. Willmann, *CrystEngComm*, 2013, **15**, 3664-3671.

29 M. Duttine, D. Dambournet, N. Penin, D. Carlier, L. Bourgeois, A. Wattiaux, K.W. Chapman, P.J. Chupas, H. Groult, E. Durand, A. Demourgues, *Chem. Mater.*, 2014, **26**, 4190-4199.

30 Y. Calage, M. Leblanc, G. Ferey, F. Varret, *J. Magn. Magn. Mater.*, 1984, **43**, 195-203.

31 M. Leblanc, R. De Pape, G. Ferey, J. Pannetier, *Solid State Commun.*, 1986, **58**, 171-176.

32 T. Krahl, F. M. Winkelmann, A. Martin, N. Pinna, E. Kemnitz, *Chem. Eur. J.*, 2018, **24**.

33 D. Dambournet, K.W. Chapman, M. Duttine, O. Borkiewicz, P.J. Chupas, H. Groult, *ChemistryOpen*, 2015, 443-447.

34 M. Burbano, M. Duttine, B.J. Morgan, O.J. Borkiewicz, K.W. Chapman, A. Wattiaux, A. Demourgues, H. Groult, M. Salanne, D. Dambournet, *J. Phys. Chem. Lett.*, 2019, **10**, 107-112.

35 Z. Yang; Z. Zhang, Y. Yuan, Y. Huang, X. Wang, X. Chen, S. Wei, *Current Applied Physics*, 2016, **16**, 905-913.

36 S. Wei, X. Wang, R. Yu, R. Zhang, M. Liu; Z. Yang, H. Hu, *J. Alloys Compd.*, 2017, **702**, 372-380.

37 Z. Zhang; Z. Yang; Y. Li; X. Wang, *J. Phys. Chem. Solids*, 2018, **123**, 87-96.

Published on 13 May 2020. Downloaded by Uppsala University on 5/14/2020 8:40:24 AM.

Dalton Transactions Accepted Manuscript

38 J. Ding, X. Zhou, H. Wang, J. Yang, Y. Gao, J. Tang, *ACS App. Mater. & Inter.*, 2019, **11**, 3852-3860.

View Article Online
DOI: 10.1039/D0DT01310B

39 Y. Lu; S. Huang, Z. Zhang, X. Huang, L. Lan, L. Lu, S. Li, J. Li, C. Pan, F. Zhao, *Ionics*, 1-8.

Published on 13 May 2020. Downloaded by Uppsala University on 5/14/2020 8:40:24 AM.

Dalton Transactions Accepted Manuscript

View Article Online
DOI: 10.1039/D0DT01310B

The first mixed iron vanadium hydroxyfluoride ($(Fe_{0.53}V_{0.47})F_{2.67}(OH)_{0.33}$) with a Hexagonal Tungsten Bronze (HTB) network was synthesized. The HTB structure possesses 1D channels allowing lithium insertion and recovering. Its electrochemical evaluation as positive electrode reveals a capacity of 181 mAh.g^{-1}. Unlike pure iron hydroxyfluoride ($FeF_{2.66}(OH)_{0.34}$) the HTB network is partially maintained upon cycling.

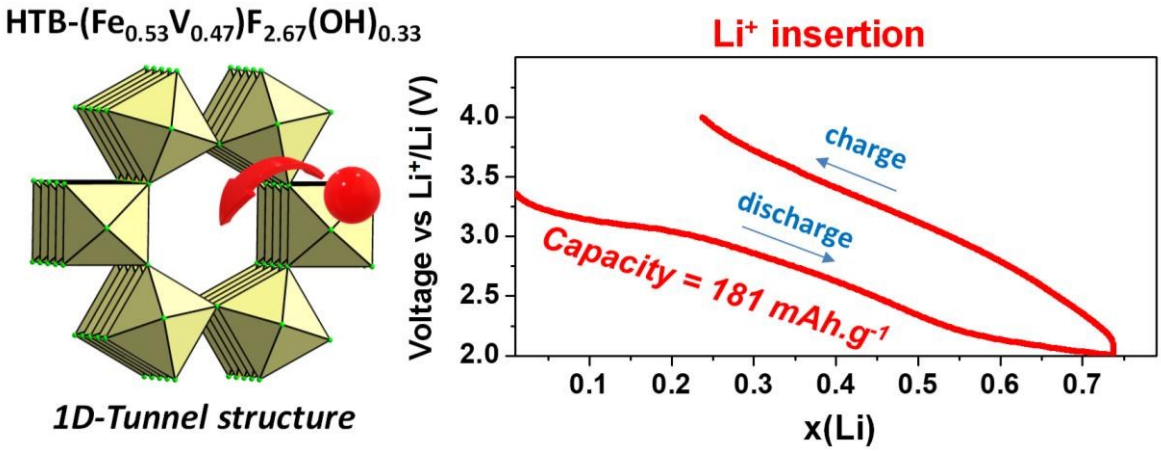

Published on 13 May 2020. Downloaded by Uppsala University on 5/14/2020 8:40:24 AM.

Dalton Transactions Accepted Manuscript